



Testing Core Loss for Rectangular Waveforms

February 7, 2010

Charles R. Sullivan

John H. Harris

Thayer School of Engineering at Dartmouth

charles.r.sullivan@dartmouth.edu

<http://engineering.dartmouth.edu/inductor>

8000 Cummings Hall

Hanover, NH 03755, USA

Edward Herbert

closs@eherbert.com

<http://fomt.com/>

1 Dyer Cemetery Road

Canton, CT 06019, USA

Sponsored by

The Power Sources Manufacturers Association

email: power@psma.com

<http://www.psma.com/>

P.O. Box 418

Mendham, NJ 07945-0418

Tel: (973) 543-9660

Fax: (973) 543-6207

Summary

In this project we have explored the feasibility of a method to generalize square-wave core-loss data to predict core loss with any common rectangular voltage waveform, proposed by Herbert [1].

The hypotheses to be tested is that, for rectangular pulses and a given magnetic core material, the core loss energy per period depends only on component pulse widths and peak voltages. We call this the *composite waveform hypothesis*. It has great intuitive appeal, and if true, it makes it convenient to decompose rectangular waveforms into such pulses for analysis. Thus, it would be sufficient to test cores with square voltage waveforms, and then use the data to predict losses with generalized rectangular voltage waveforms.

Two important objectives of the project are to

1. Gather such square wave data for two typical core materials, one ferrite and one powdered-iron.
2. Gather additional data to determine if the composite waveform hypothesis is valid.

The square wave data were gathered for a set of data points at intervals that would be practical for manufacturers to provide for designers—five values per decade for both peak voltage and pulse width.

The validation data were measurements for non-square-wave composites of “standard” pulses from the square wave data set. We used three variations: (1) symmetric waveforms formed from a standard pulse shape with varying amounts of off-time added, increasing the period, (2) families of standard pulse shapes with set off-time, but varying the asymmetry, and (3) asymmetric waveforms with no off time, formed from two different standard pulse shapes.

It was clear from the large size of the sample space implied by this program, that an automated data gathering system would be needed, so computer control was designed in from the start. A data management system evolved that can generate a set of control input parameters for the test setup for all data points from a few global parameters, and then analyze the results.

The drive circuitry was designed to cover a wide range of flux density and frequency, consistent with budget constraints, by using existing experimental circuit boards.

The results indicate that the composite waveform hypothesis, while not perfect, performs well, and should be a significant improvement over the use of sinusoidal data for PWM design. The deviations from composite waveform model may provide valuable insight into the loss processes, and future work to characterize this behavior can likely improve the model and its value for design.

Contents

1	Introduction	1
2	Previous Methods for Core Loss with Non-sinusoidal Waveforms	1
3	Calculating Core Loss from a Simplified Data Set	3
4	Measurement System	4
4.1	Data Flow	6
4.2	Preferred Values	7
5	Experimental Results	8
5.1	Characterization	8
5.2	Verification	9
6	Hysteresis Loops	16
7	Design Techniques	17
8	Discussion	21
9	Using the Data	22
10	Conclusion	22
A	Data Files and Fields	24
A.1	Oscilloscope Data	24
A.2	Test Input Data	25
A.3	Run Data Generator	26
B	General File Formats	27

List of Figures

1	Waveform types.	3
2	Full-bridge excitation circuit.	5
3	Decoding waveforms.	5
4	Block diagram of the experimental apparatus.	7
5	Experiment data flow.	8
6	Square-wave loss data, ferrite core.	10
7	Square-wave loss data, powdered-iron core.	11
8	Losses with asymmetric waveforms.	12
9	Test data for waveform with off time, ferrite core.	13
10	Test data for waveform with off time, powdered iron core.	14
11	Hysteresis plots for expand data set, $t_1 = 3.98 \mu s$	15
12	Hysteresis plots for expand data set, $t_1 = 6.31 \mu s$	16
13	Hysteresis plots for expand data set, $t_1 = 10 \mu s$	17
14	Zoomed in hysteresis plots for expand data set, $t_1 = 3.98 \mu s$	18
15	Reading a Herbert plot.	19
16	Design example.	20

List of Tables

1	Devices for the Drive Circuitry.	6
2	Sample cores.	8
3	File naming conventions for parameter and data files.	24
4	Waveform type designations	25

Preface

Most of the content of this report was taken from a paper to be published in the proceeding of the IEEE Applied Power Electronics Conference for 2010. I have added more detailed information the help with a practical understanding of the data gathering system and the use of the data.

John H. Harris

1 Introduction

Core-loss data published by core manufacturers is based on sinusoidal excitation, whereas most applications in switching power supplies and other types of power electronics circuits use rectangular voltage waveforms. Rectangular waveforms can be described by the voltage, period, and duty cycles of the positive and negative portions of the waveform. This leads to a wide diversity of different possible test conditions, and it is not practical for manufacturers to test all possible waveforms that might be used by customers. Approximate methods to estimate expected core loss with rectangular waveforms based on sinusoidal data [2]–[9] exist, but are difficult to use, are inherently limited in accuracy, and are not in wide use in industry.

In this project, we investigate a new approach that uses a simplified set of square-wave measurements to produce easy-to-use data that can be applied to calculate loss for any rectangular-voltage waveform. This approach is expected to provide higher accuracy than is possible starting from data based on sinusoidal waveforms, and is expected to be easier to use than existing methods for non-sinusoidal waveforms. The method can be applied to computerized optimizations or in hand calculations using graphical data. Although the data required is different from conventional sinusoidal measurements, the amount of data needed is no more than the amount of data collected in traditional loss characterization.

In order to implement and evaluate the new method, we have developed an automated excitation and data collection system under computer control. This allows rapidly gathering the proposed square-wave characterization data set, and also facilitates scanning through other rectangular waveform sets in order to assess the accuracy of the generalization from the characterization data.

Previous methods for predicting core loss with rectangular waveforms based on sinusoidal data are reviewed in Section 2. The new calculation method is described in Section 3 and the measurement system in Section 4. Measurement results are presented and used to assess the accuracy of the method in Section 5. Hysteresis loops are plotted and discussed in Section 6. A guide to applying the method in practical design is provided in Section 7. Section 8 further discusses the future application and improvement of this approach. Section 9 discusses the use of the accompanying data sets, and the appendix gives detailed information about data file formats.

2 Previous Methods for Core Loss with Non-sinusoidal Waveforms

For sinusoidal waveforms, loss is often estimated by a power law equation [10, 11]

$$\overline{P}_v = k f^\alpha \hat{B}^\beta \quad (1)$$

where \hat{B} is the peak flux amplitude, \overline{P}_v is the time-average power loss per unit volume, and f is the frequency of sinusoidal excitation, and k , α , and β are constants found by curve fitting. A similar equation, but without the frequency dependence, was proposed by Steinmetz in 1892 [12], and so (1) is often referred to as the Steinmetz equation.

Unfortunately, the Steinmetz equation, as well as the data provided by manufacturers of magnetic materials, is based only on sinusoidal excitation, and non-sinusoidal waveforms result in different losses [2, 3, 6]. DC bias can also significantly affect loss [13, 14, 15].

More detailed models, based on physical phenomena producing loss, have been studied [16]–[19].

However, especially for ferrites, there is not yet a clear consensus on a practical physically-based model that properly includes dynamic and nonlinear effects [6].

Initial attempts to make use of Steinmetz-equation parameters and extend the calculation to address arbitrary waveforms allowed improved loss estimates, but have significant limitations. The “modified Steinmetz equation” (MSE) [2, 3, 4] works well for waveforms with small harmonic content, but exhibits anomalies with large harmonic content [6], as does the model introduced in [5], as discussed in [7]. The “generalized Steinmetz equation” (GSE) was introduced in [6] to overcome anomalies in the MSE, and although it overcomes the problems with the MSE, it has poor accuracy in some regions [7].

A satisfactory method of using Steinmetz-equation parameters to roughly estimate loss with non-sinusoidal waveforms, the “improved generalized Steinmetz equation” (iGSE) was introduced in [7]. The same equation was independently discovered in [8, 9], where it was called the natural Steinmetz extension (NSE). Comparisons of different approaches in [25] confirm results in [7, 8, 9] showing that this method can work well in many situations.

An additional refinement introduced in [7] is to decompose a waveform that includes minor loops in the hysteresis curve, and separately analyze the loss in each minor loop. This was shown to be essential for accurately modeling such cases. An automated algorithm is described in [7] to perform this decomposition, but is unnecessary for waveforms without minor loops.

Despite these improvements, the iGSE remains an approximate prediction method, and, in particular, is dependent on the accuracy of the underlying Steinmetz model for sinusoidal loss. Unfortunately, the best-fit Steinmetz parameters are known to vary with frequency [26, 6]. For waveforms with a harmonic content over a wide frequency range, choosing the appropriate parameters can be problematic [6]. Some solutions to this problem that work for sinusoidal waveforms (e.g., [26, 27]) are not applicable with the iGSE. Summing several power-law terms is one option that can be used to better capture the wide-range frequency behavior while retaining compatibility with the general approach of the iGSE, at the price of additional complexity [8].

The approach in this project is to directly measure loss with square waveforms, rather than trying to extend data from sinusoidal loss measurements to square waveforms. The advantages relative to the iGSE and related methods are both simplicity and accuracy. The challenge to developing such a method is to be able to take data for a reasonably constrained set of parameters, and be able to use the results to predict loss for a wider range of practical waveforms. This is discussed in the next section.

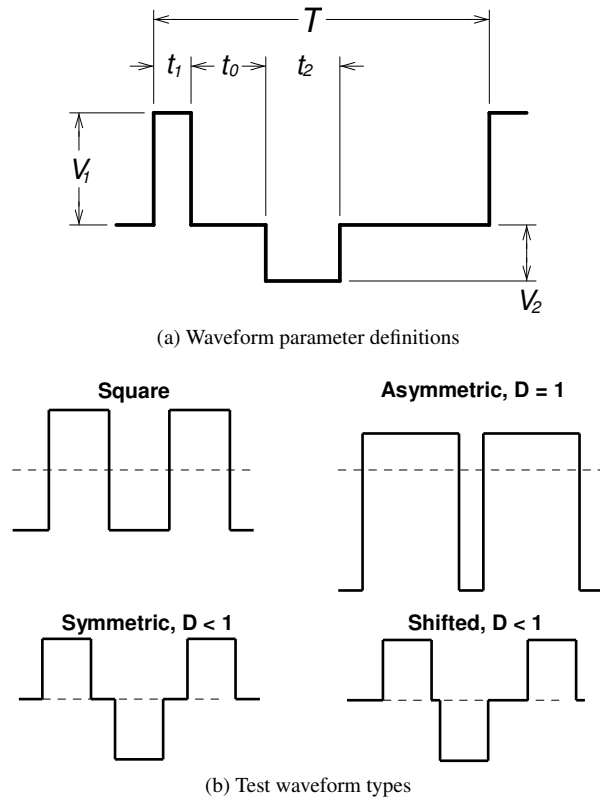


Figure 1: Waveforms (voltage vs. time): parameters and test waveform types. Square waves are used for characterizing materials; the other test waveforms are used to test the validity of the composite waveform hypothesis.

3 Calculating Core Loss from a Simplified Data Set

Consider a core with voltage waveforms such as those shown in Figure 1, typical of power electronics applications, applied to a winding. The flux in the core will ramp up or down during each positive or negative voltage pulse, respectively. We hypothesize that the energy loss incurred during each of these flux transitions depends only on the amplitude and duration of the pulse, and that there is no loss during periods of zero applied voltage (constant flux). If this is the case, we can decompose any of the rectangular waveform types shown in Figure 1b into a set of two pulses, calculate the energy loss associated with each pulse, and sum them to find the total energy loss per cycle. We call this hypothesis the *composite waveform hypothesis*.

If the composite waveform hypothesis proves to be a good approximation, we can predict core loss for any of the waveforms in Figure 1b if we know the loss for a square pulse as a function of its amplitude and duration. While we might estimate that loss

from sinusoidal data using one of the methods describe in Section 2 ([2]–[9]), a more accurate approach is to collect measured test data with square voltage waveforms, for which we can assume that the loss associated with each pulse is one half of the per-cycle energy loss. This requires data as a function of two parameters, such as flux amplitude and frequency, as used in conventional sinusoidal loss characterization. The parameters may also be described in terms of applied voltage per turn (corresponding to flux ramp rate) and on-time t_1 (one half the period for square waves).

The method we propose starts with characterizing a core material by measuring loss data for square waveforms. One half of the measured energy loss per cycle is the energy lost for a single pulse of the applied amplitude and on-time. If the composite waveform hypothesis is accurate, the same loss per cycle will be incurred for that applied voltage and on-time in any composite waveform. For the waveforms we consider here (Figure 1), the waveform comprises two pulses. To find the total energy loss per cycle one sums the per-pulse loss data for each of the two sets of pulse parameters (amplitude and on-time) from the corresponding square-wave measurements.

In Sections 4 and 5 we report on experimental measurements conducted for two purposes: (1) to collect square-wave data for sample cores as is necessary for this method, and (2) to assess the accuracy of the method and of the composite waveform hypothesis. We note that all of the previous methods for predicting loss with non-sinusoidal waveforms discussed in Section 2 depend on some version of the composite waveform hypothesis, even though this assumption is rarely stated. Thus, tests of this hypothesis are important for other approaches to predicting non-sinusoidal losses as well as for validating the approach proposed here.

Predictive core loss models built up from fundamental physical principals are not available for most core loss mechanisms, and so theoretical analysis of the composite waveform hypothesis is not possible. However, for core loss produced purely by classical eddy-current effects, physical models are well established, and analytical solutions exist for some geometries. It can be shown that, for classical eddy-current loss in core material layers thicker than or comparable to an electromagnetic skin depth, the composite waveform does not always hold exactly. However, it may still be a useful approximation, and may hold exactly for other types of losses. Thus experimental evaluation is needed to assess its utility.

4 Measurement System

We use a two-winding loss measurement [9] on toroidal core samples with 5 or 21 turns to match core characteristics to our drive system capabilities. The drive winding is connected to a full-bridge switching network through a $320\ \mu\text{F}$ blocking capacitor (Figure 2). The gates of the four MOSFETs are controlled by an Agilent 33220A arbitrary waveform generator through a logic circuit and optically isolated gate drivers. Both the arbitrary function generator and the DC power supply feeding the bridge circuit are automatically controlled by a computer to allow synthesis of a sequence of different rectangular voltage waveforms. The principle components used in the circuit are summarized in Table 1.

The Agilent waveform generator has only one arbitrary waveform output (labeled

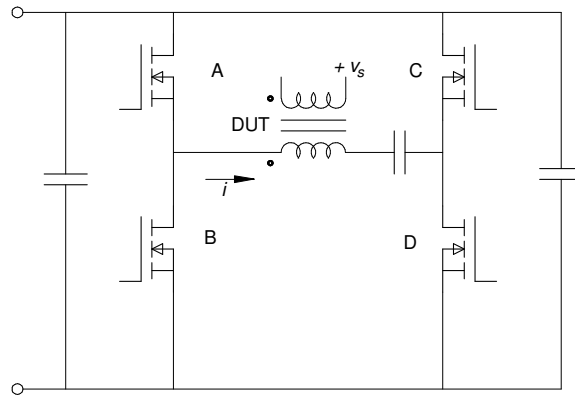


Figure 2: Full-bridge excitation circuit. The device under test, a magnetic core, is labeled DUT.

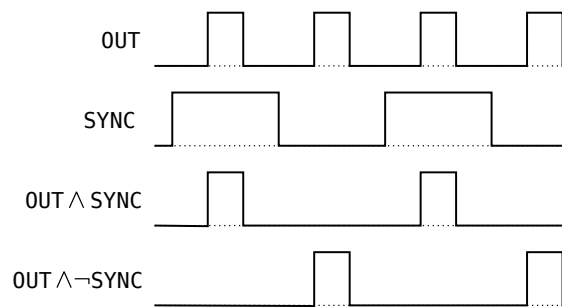


Figure 3: Decoding two drive signals from the OUT and SYNC waveform generator outputs.

OUT), but we have two phases of the bridge to be driven. We could generate a bipolar, three-level output from the arbitrary output, but then we would be using an analog representation of an essentially digital phenomenon, which introduces unnecessary trimming and level-shifting design compromises. Instead, by using a properly chosen OUT signal, gated with the generator's TTL square wave synchronization output (SYNC), we can get two independent but synchronized digital pulse trains: one is $OUT \wedge SYNC$, the other $OUT \wedge \neg SYNC$ (Figure 3). This is accomplished with just a few logic gates, and can produce all of the $D < 1$ waveforms. The asymmetric $D = 1$ waveforms can be generated with the same gates by switching to the OUT signal alone (i.e., holding SYNC high). The square wave can be made several different ways; we use holding OUT high, which gives SYNC and $\neg SYNC$.

Dead time protection is hardwired for reliability. The dead-time circuits are hand-trimmed to get optimal waveform fidelity.

Current in the drive winding is sensed with an Agilent DSO 7104A oscilloscope with a Tektronix P 6021 wideband passive AC current probe. The AC probe avoids the

Table 1: Devices for the Drive Circuitry.

Function	Description	Value
Power supply.	Sorenson XG33-25	33 V, 25 A
Switching MOSFET.	IR IRF 3706	20 V, 77 A
Opto-isolated gate drive.	Avago HCPL-3180	2.5 A, 250 kHz
Blocking capacitor.	AVX FFV3	$2 \times 160 \mu\text{F}$
Power supply decoupling capacitor, high capacity.	electrolytic	$2 \times 120 \text{ mF}$
Power supply decoupling capacitors, low Z .	X7S surface mount	$10 \times 10 \mu\text{F}$

delay inherent in an active current probe; delay measurements verify that the delay is negligible. Flux is calculated from the voltage v_s across a sense winding. These signals are acquired by a digital storage oscilloscope under computer control to automatically collect waveforms from a sequence of measurements. After the waveforms are allowed to reach steady-state, 512 periods are averaged, and the average is recorded with 1000 points per period. Core loss and other parameters are calculated off line from the acquired data.

The core temperature was controlled by immersion in a heated oil bath. All the results reported here are for an oil-bath temperature of 80°C . The automated data collection allows acquiring data for a single excitation in less than two seconds; a pause of about two seconds precedes the next excitation. Even without the oil bath, this results in very little temperature rise; with the oil bath, temperature deviations are negligible.

For verification of the test system, a large air-core toroidal transformer was constructed. This would, in principle, provide a zero-core-loss reference. However, large stray capacitance in the transformer led to excessive ringing in the waveforms and negative power dissipation numbers. Future work will develop a better reference design to allow a useful air-core test.

4.1 Data Flow

The data were generated using an automated system (Figure 4). The apparatus is controlled, via a local area network (LAN), by a program named *Coreloss*, which has a graphical user interface. It is the experimenters primary interface with the setup.

Initially, the experimenter edits a file describing a batch of runs in terms of a few general parameters, using a text editor. This is processed by a program named *Genruns*, that generates a table of run parameters defining the setup of the experimental apparatus for each run. This file can be opened from the *Coreloss* program and the user can execute any single run (For exploratory work, single runs can be edited before running), or all the runs can be executed sequentially and automatically. All the square wave data used to characterize a given core can be gathered in about half an hour. Further processing of the raw data is accomplished off line.

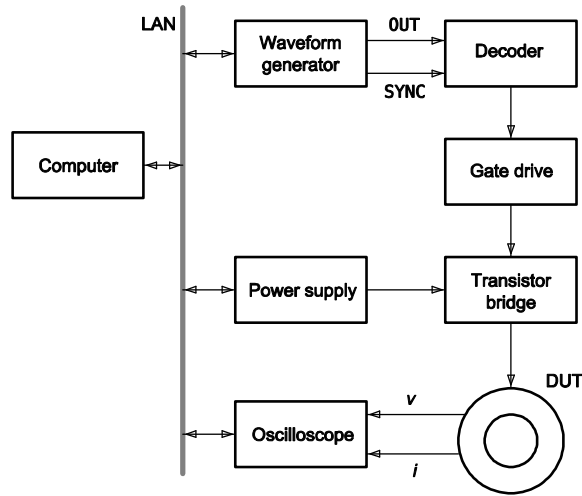


Figure 4: Block diagram of the experimental apparatus.

An experimental *run* is a data sample of one waveform shape, with a given t_1 , T , V_{ps} , and perhaps other parameters, depending of the type of waveform. Experimental runs are grouped in *families*, several runs that vary one parameter while holding others constant.

A number of files are generated in the process of conducting the experiments. Figure 5 is a Petri diagram of the information flow. For the sake of data management, runs are also grouped in *sets*. A set is a batch of runs described in a single data file with the name `set-gen.dat`, where *set* is the set identifier.

The Gen-runs program reads the input data set file, and creates a file named `set-runs.dat`, a table which describes each individual run, to be read by the Coreloss program, which operates the apparatus. Each run has a run ID number. The oscilloscope, under computer control, measures the resulting voltage and current data, and records it in files named `set-run.csv`, where *run* is the run number. These CSV files are the raw data for the experiment.

There are other files that provide diagnostic information. The files names and field names and their interpretation are presented in Appendix A. The file formats are described in Appendix B.

4.2 Preferred Values

In order to make the data easier to plot and use, we chose values of voltage-per-turn and pulse width in geometric series. The software application programming interface (API) deals with integer *decilogs*—integer values of $10 \log_{10} x$ (i.e., like decibels, but not restricted to power measurements). Our reference levels are 1 volt per tune, and 1 ampere. For the present project, points were even-integer decilog values, corresponding to the sequence $x = \{1, 1.58, 2.51, 3.98, 6.31, 10\}$. Note that we chose excitation voltages to be preferred *per-turn* values, so that data could be compared for coils with

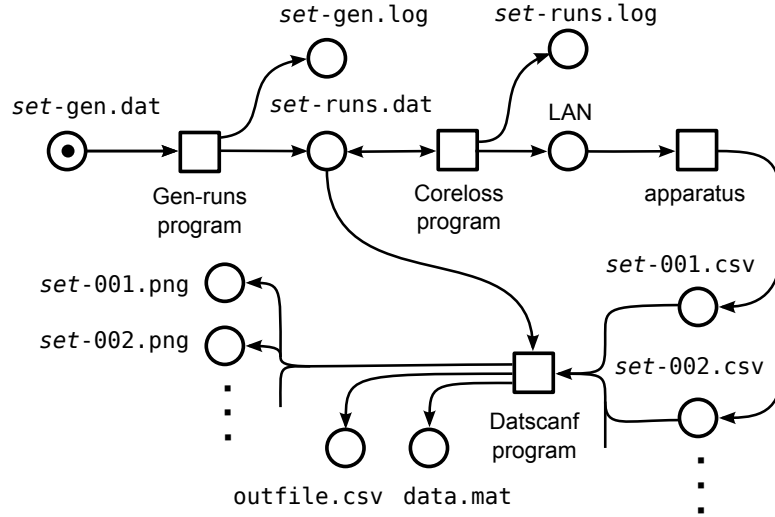


Figure 5: Petri diagram of the experiment data flow. Circles are channels (files or network), boxes are processes.

Table 2: Sample cores.

Manufacturer	Part	Material	Turns, N
Magnetics	42206-TC	R ferrite	5
Micrometals Inc.	T80-52	-52 iron powder	21

differing N —the preferred values above may be hidden behind a factor of N .

5 Experimental Results

Two sample cores were tested: one ferrite core and one powdered-iron core, as listed in Table 2.

5.1 Characterization

Figure 6 presents square-wave loss data in two different formats for the ferrite core. Figure 6a uses a format similar to that used for sinusoidal loss data on many datasheets. Figure 6b shows a Herbert curve in which core loss is plotted as a function of on-time (t_1 in Figure 1a), parameterized by the voltage per turn during that on-time [1]. The Herbert curve is convenient for use in design as discussed in Section 7; in addition, it directly illustrates the effect of period on power loss and can help guide the choice of switching frequency. Starting at a low switching frequency, increasing frequency (and thus reducing the pulse width) decreases losses, but beyond a certain frequency, further increases not only result in diminishing returns, but actually increase core losses. This

point corresponds to pulse widths of 1.5 to 3 μs for the ferrite material tested, and thus periods of 3 to 6 μs , and square-wave frequencies of 167 to 333 kHz. This is generally consistent with the behavior seen in plots of “performance factor” $B \cdot f$ for fixed power loss provided by some manufacturers [28, 29, 30]. However, the frequency beyond which performance degrades is lower in our data than in plots of performance factor for the same material (about 600 kHz [28]), presumably because of the harmonic energy content of the square-wave excitation.

Square-wave loss data for the powdered-iron core is shown in the same two formats in Figure 7, and shows similar trends though the values are different.

5.2 Verification

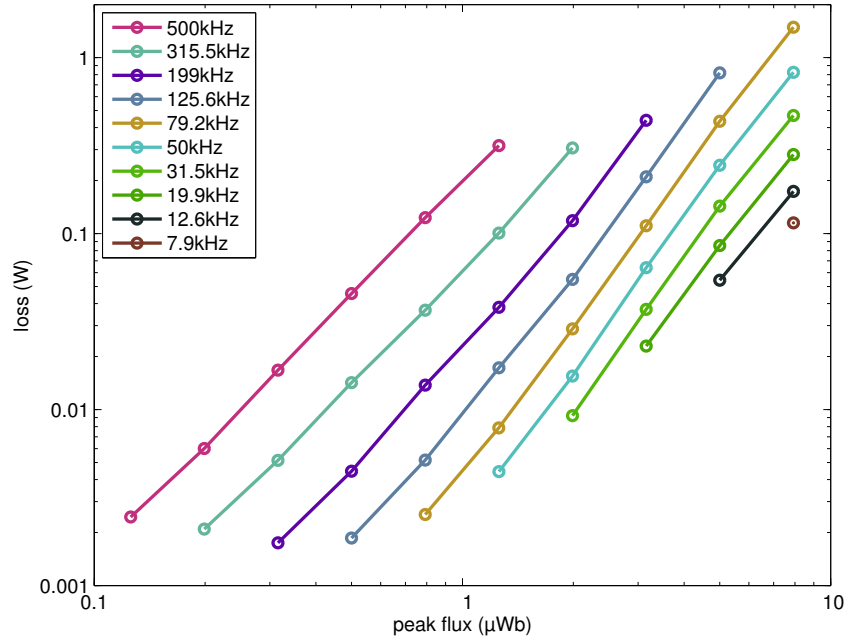
Additional data was collected to assess the accuracy of the method described in Section 3 for predicting loss for other waveforms using only data from square-wave measurements. The first category of these tests is experiments using asymmetric waveforms as shown in Figure 1b (upper right). The results of these experiments are plotted in Figure 8. Each curve is for fixed width and amplitude of the first pulse (fixed V_1 and t_1 as defined in Figure 1a) with the width of the second pulse (t_2) varying. The amplitude of the second pulse was adjusted for zero average voltage. The widths and amplitudes were all chosen to match data in the original characterization data set such that no interpolation was needed to predict loss, and the energy loss per cycle could be predicted from two points in the characterization data: the energy loss per cycle for a square wave of amplitude V_1 and half-period t_1 ($E_{\text{sqw}}(V_1, t_1)$) and the energy loss per cycle for a square wave of amplitude V_2 and half-period t_2 , as

$$E_c = \frac{1}{2} (E_{\text{sqw}}(V_1, t_1) + E_{\text{sqw}}(V_2, t_2)) \quad (2)$$

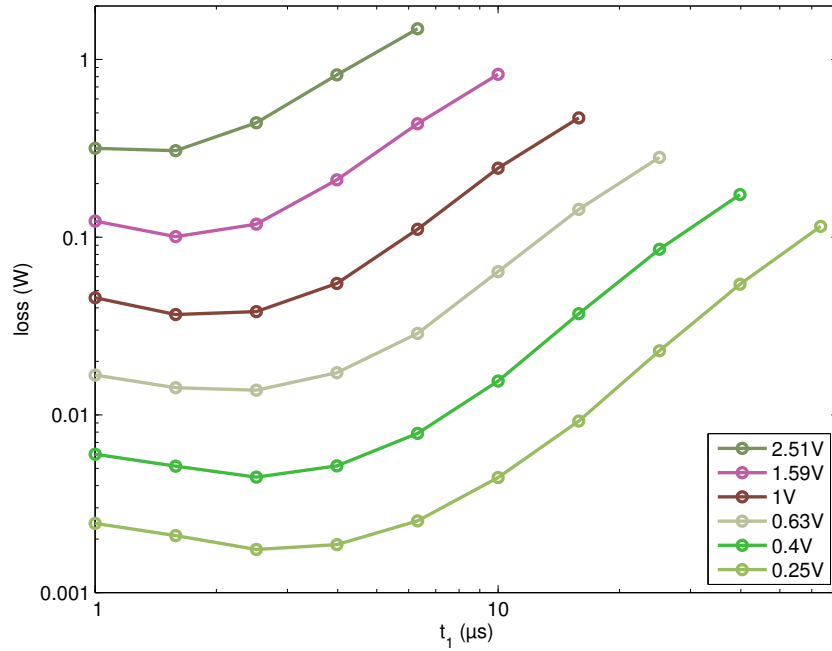
The measured asymmetric waveform loss is compared to loss predicted from (2) in Figure 8, showing excellent matching over a wide range of asymmetry ratios (t_1/T) and amplitudes, for both the ferrite core and the powdered iron core. This confirms that the composite waveform hypothesis is a good approximation for asymmetric waveforms.

Test results for waveforms with a zero-voltage time t_0 between pulses are shown in Figures 9 and 10. In each test, the positive and negative voltage pulses have constant amplitude and duration (as listed in the figure legend), but the zero-voltage time between pulses, t_0 , is varied. In Figures 9a and 10a, the waveform is always symmetric and the overall period is expanded as t_0 is increased (marked “Symmetric, $D < 1$ ” in Figure 1b). In Figures 9b and 10b, the period remains constant but the waveform is skewed with one of the two zero-voltage periods shrinking as the other expands (marked “Shifted, $D < 1$ ” in Figure 1b).

Based on the composite waveform hypothesis (see Section 3), we would expect Figures 9a and 10a to show constant energy loss per cycle as the zero-voltage time, and thus the period, increases, with no loss occurring during the zero-voltage time. The data in Figure 9a, for the ferrite core, show significant variations as t_0 increases, as much as about 40%, in some cases increasing and in others decreasing. The data in Figure 10a, for the powdered-iron core, show much less variation, matching the expectation from

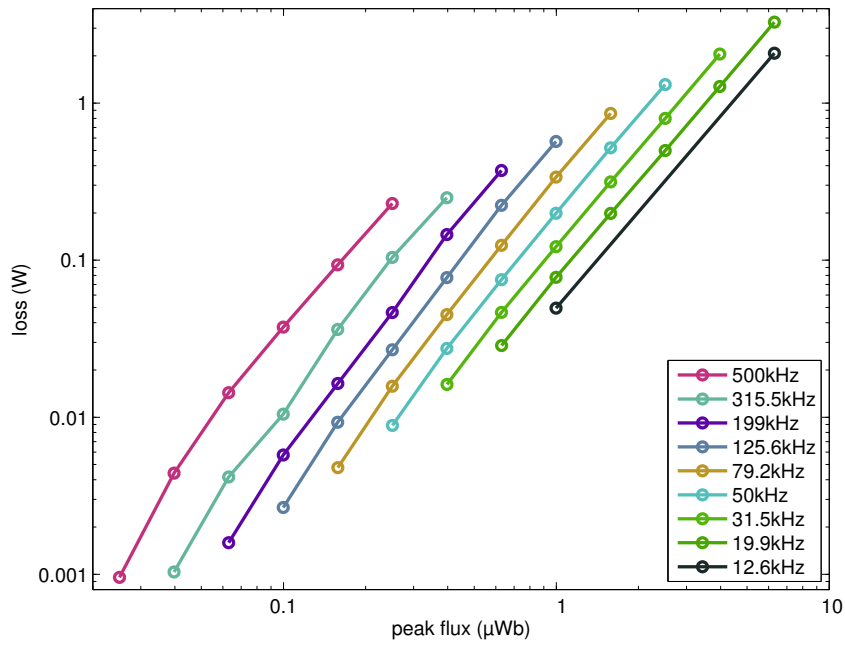


(a) Loss vs. peak flux parameterized by frequency

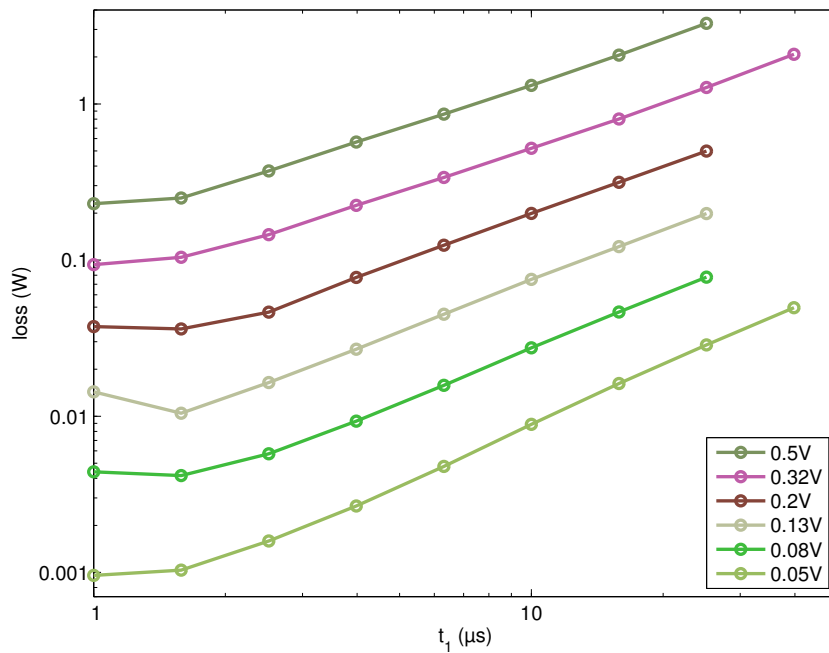


(b) Herbert curves: loss vs. on-time parameterized by voltage per turn

Figure 6: Square-wave loss data for the ferrite core in Table 2 presented in two different formats.

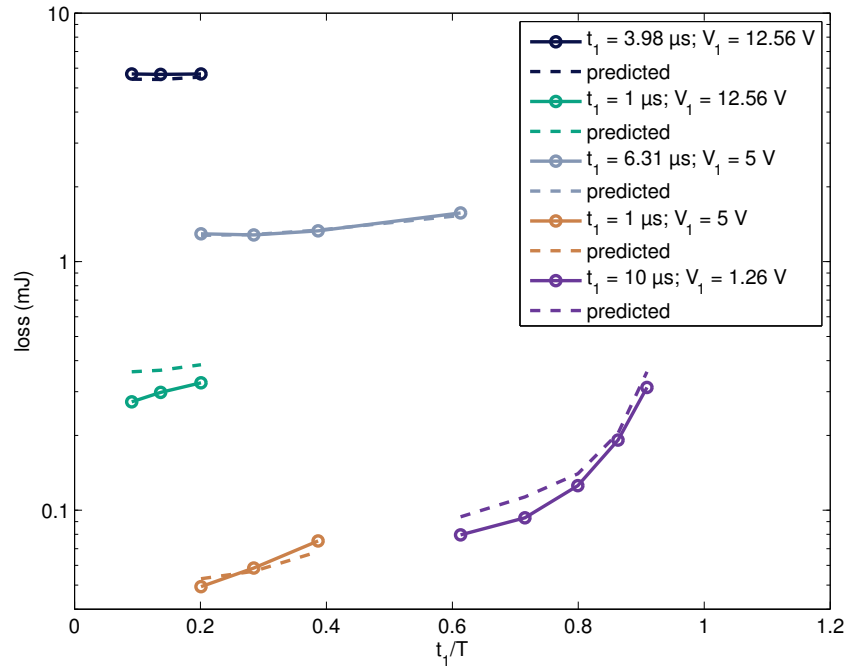


(a) Loss vs. peak flux parameterized by frequency

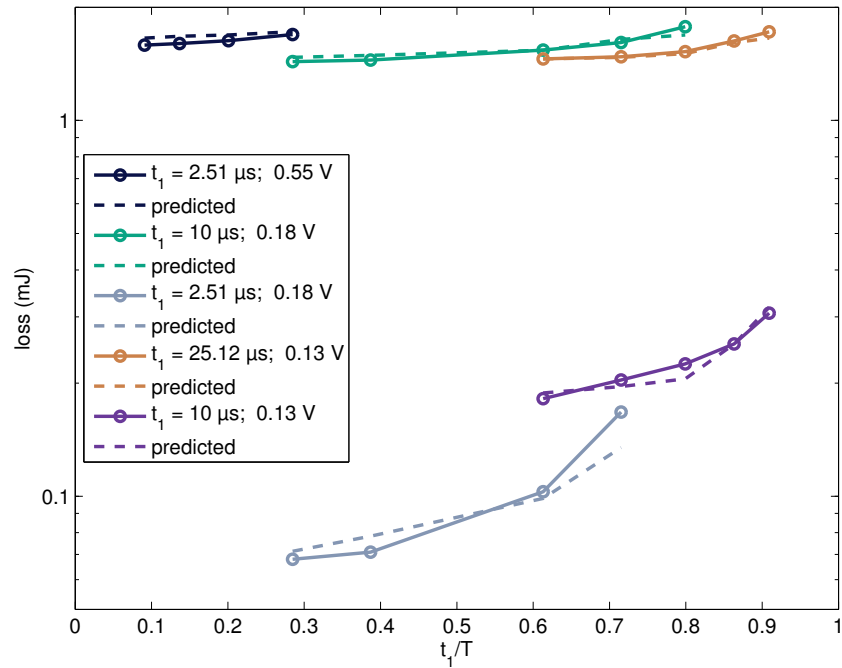


(b) Herbert curves: loss vs. on-time parameterized by voltage per turn

Figure 7: Square-wave loss data for the powdered-iron core in Table 2 presented in two different formats.

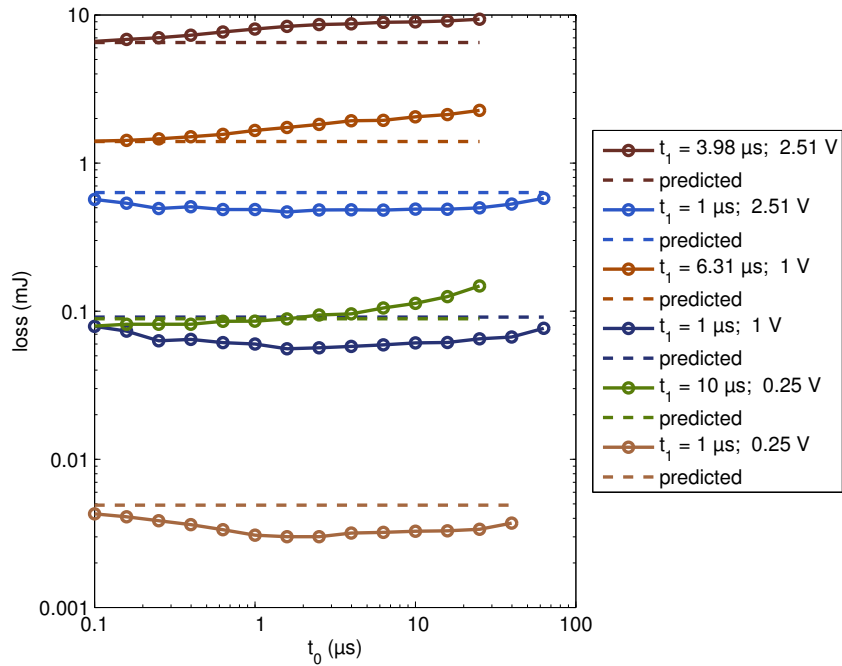


(a) Ferrite Core

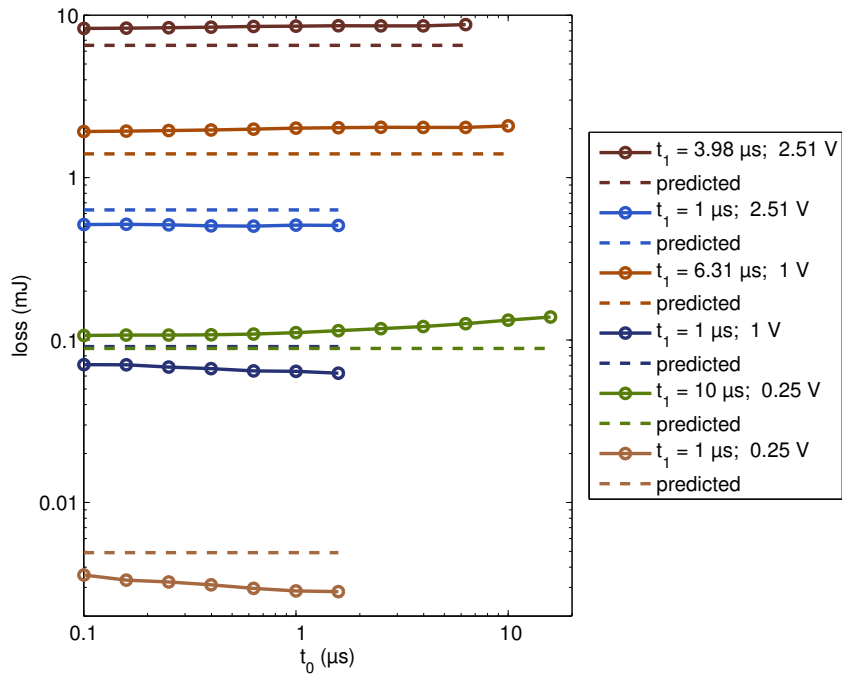


(b) Powdered-Iron Core

Figure 8: Losses with asymmetric waveforms as predicted by the proposed approach compared to measured results.

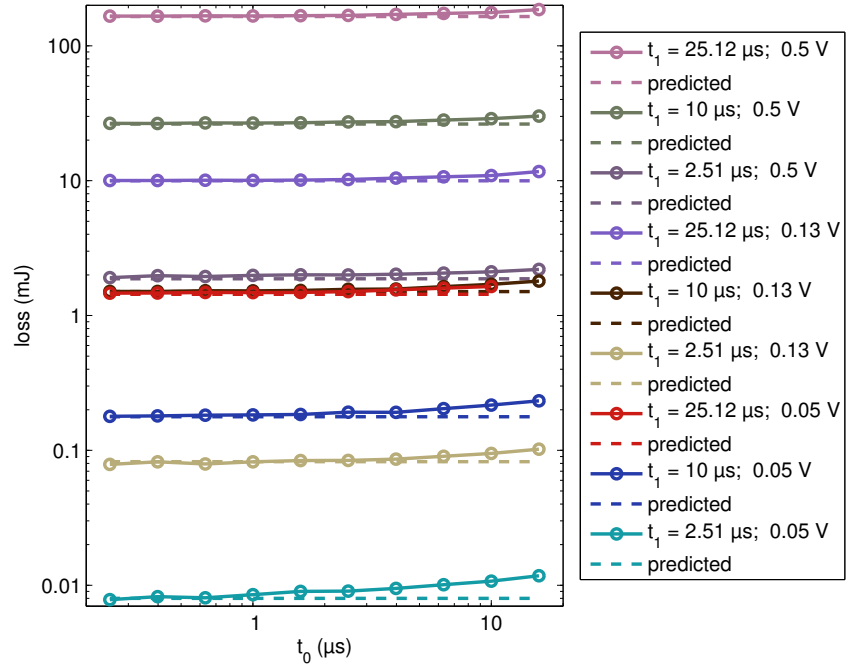


(a) Varying period

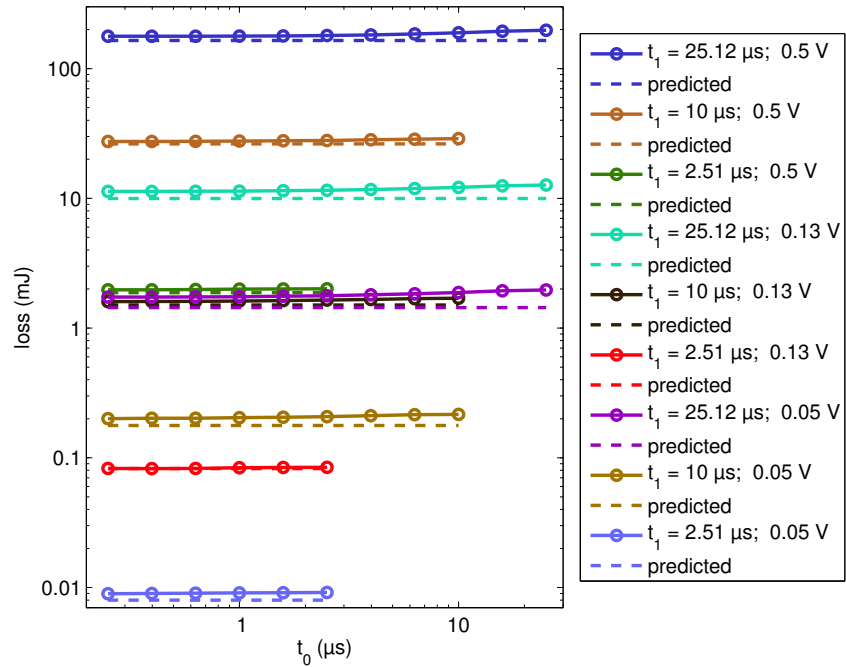


(b) Imbalanced off-times

Figure 9: Experimental data testing the extension of ferrite-core square-wave data to waveforms incorporating zero-voltage time t_0 . This is done by varying the period and extending off-time t_0 , or by shrinking one zero-voltage time while expanding the other to maintain a constant period. The legend gives the on-time t_1 and the per-turn pulse voltage for each curve.



(a) Varying period



(b) Imbalanced off-times

Figure 10: Experimental data testing the extension of powdered-iron-core square-wave data to waveforms incorporating zero-voltage time t_0 . This is done by varying the period and extending on-time t_1 , or by shrinking one zero-voltage time while expanding the other to maintain a constant period.

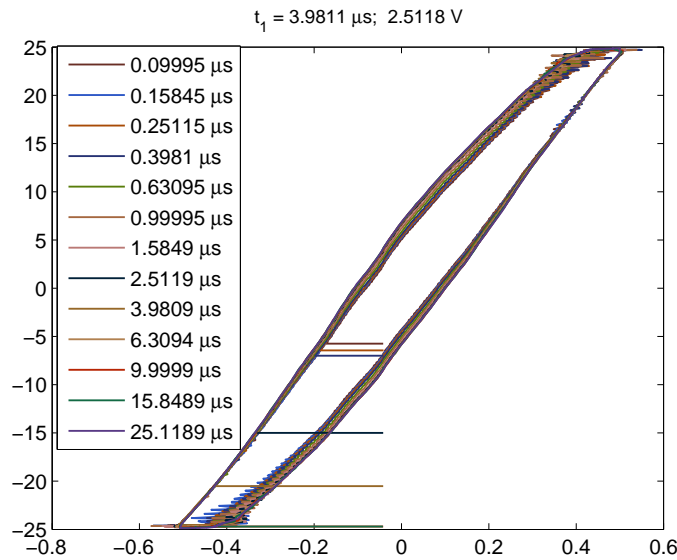


Figure 11: Hysteresis loops for one data set in Figure 9a: the top curve for $t_1 = 3.98 \mu\text{s}$. The legend shows t_0 for each loop, corresponding to one data point on the top curve in Figure 9a.

the composite waveform hypothesis very closely, with only slight increases in loss for long off-times, which may be a result of measurement artifacts.

The results for the shifted pulse waveforms, in Figures 9b and 10b, show little variation in loss as the pulse position is shifted (increasing one off-time while decreasing another), as would be expected from the composite waveform hypothesis, but the ferrite-core loss is slightly different from that predicted from the square-wave characterization data using (2), whereas the powdered-iron core matches the predicted loss more closely. This is consistent with the results shown in Figures 9a and 10a. For the ferrite core, the relatively low variation in loss as the pulse position shifts, compared to that shown in Figures 9a and 10a, could be explained by the effects of one off-time increasing offsetting the effect of the other decreasing for a net zero effect on loss. Alternatively, if the trends shown in Figures 9a and 10a are due to measurement artifacts associated with the expanding period, this could also explain the relatively flat behavior seen in Figures 9b and 10b, because the shifted pulse experiments are immune to any errors associated with waveform period. However, the difference in behavior between the two cores seen in Figure 9a and 10a indicates that the trends seen in the data are in fact due to the true behavior of the cores, not to any unexpected measurement artifacts.

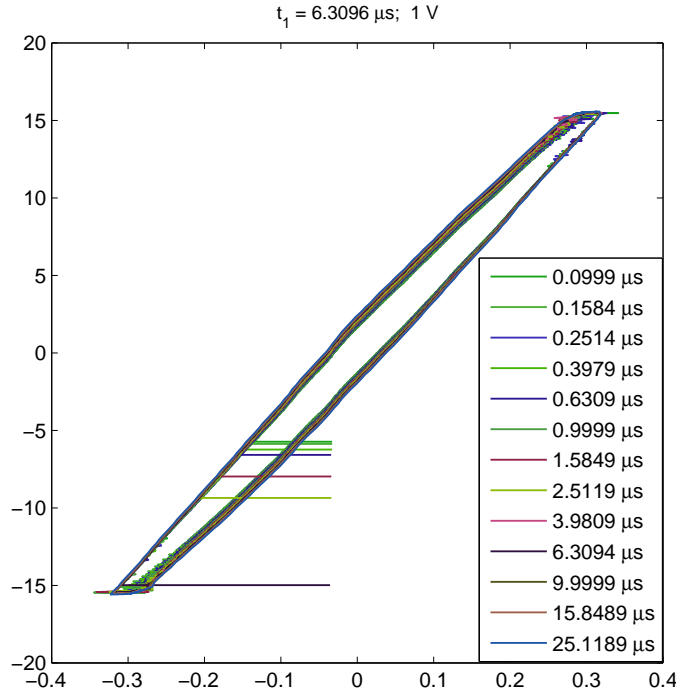


Figure 12: Hysteresis loops for one data set in Figure 9a: the second curve from the top, for $t_1 = 6.31 \mu\text{s}$. The legend shows t_0 for each loop, corresponding to one data point on the second curve in Figure 9a.

6 Hysteresis Loops

To further explore the phenomena causing variations in loss when the zero-voltage time between pulses, t_0 , is varied, hysteresis loops for each point in several of the curves in Figure 9a are plotted in Figures 11, 12, and 13.

The scale and number of curves on these figures, together with ringing on the waveforms, makes it difficult to see a dramatic trend, particularly on the relatively narrow loops of Figure 12 and Figure 13. However, a zoomed in view of Figure 11, shown in Figure 14, provides some insight. We see that the rise to the point of maximum current and flux linkage is nearly identical on each curve, with the exception of ringing that has little effect on the area of the loop. However, the decreases diverge: those with the shortest zero-voltage time t_0 fall more directly, while those with longer zero-voltage time curve further to the left. This part of the curve immediately follows the pause at zero voltage (which is at the top right of the plot), and thus it makes sense that its shape is the most affected by the pause. An oversimplified description would be that the flux gets “stuck” near the the maximum value if it has had time to “soak” and get

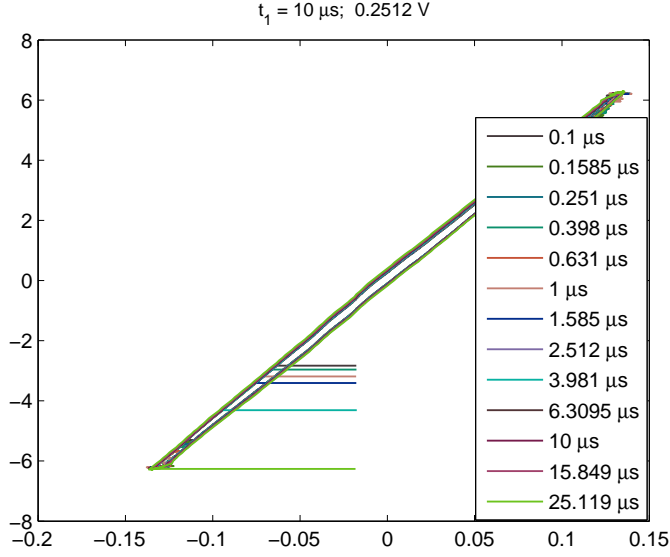


Figure 13: Hysteresis loops for one data set in Figure 9a: the fourth curve from the top, for $t_1 = 10 \mu\text{s}$. The legend shows t_0 for each loop, corresponding to one data point on the fourth curve in Figure 9a.

accustomed to that flux value, whereas the flux can more easily transition away from the maximum if the excitation is decreased immediately.

7 Design Techniques

The loss data derived from square-wave measurements can be provided to a magnetics designer in various forms, including tabulated data or curve-fit functions for use in software, and various types of graphical presentation. The loss data can be presented as loss per unit volume, or as total loss for a specific core, to simplify calculations for the designer. Here we discuss working from graphical data in the “Herbert curve” format of Figure 6b. These curves are parameterized by voltage per turn applied to a winding. It’s also possible to provide curves like this for a specific *component* with a given number of turns, parameterized by voltage.

In general, for waveforms as shown in Figure 1a, based on (2), one can calculate loss from a Herbert plot as

$$P = \frac{1}{T} (P_{\text{sqr}}(V_1/N, t_1) \cdot t_1 + P_{\text{sqr}}(V_2/N, t_2) \cdot t_2) \quad (3)$$

In the case of symmetric waveforms, $P_{\text{sqr}}(V_1/N, t_1) = P_{\text{sqr}}(V_2/N, t_2)$, and the loss calculation reduces to

$$P = \frac{2t_1}{T} P_{\text{sqr}}(V_1/N, t_1). \quad (4)$$

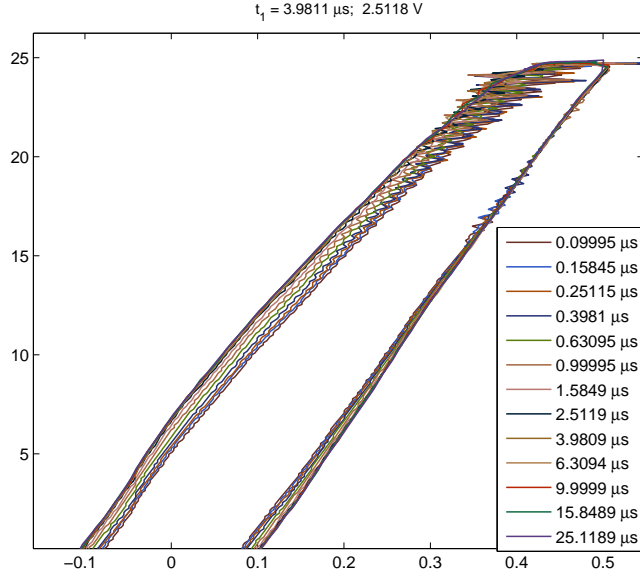


Figure 14: A zoomed-in view of the hysteresis loops in Figure 11. The legend shows t_0 for each loop, corresponding to one data point on the top curve in Figure 9a.

Consider, for example, a component operating at 50 kHz with a symmetric waveform with a duty cycle of 63%, 12 turns, and a pulse amplitude of 4.8 V. The period is 20 μs , and the positive and negative pulse widths are $t_1 = t_2 = 0.63 \cdot 10 \mu\text{s} = 6.3 \mu\text{s}$. To find the correct curve to examine in Figure 6b, we find the voltage per turn which is $4.8/12 = 0.4$ V. As shown in Figure 15, we can read off the power loss for this pulse width and voltage per turn as $P_{\text{sqr}} = 7.9$ mW. According to (4) we scale this result by the ratio $2t_1/T = 12.6 \mu\text{s}/20 \mu\text{s}$, to get a predicted power loss of $7.9 \cdot 0.63 = 5$ mW.

An interesting design space to explore is to maintain constant frequency and average voltage, but to vary the pulse width and period. The relevant data is along a curve of constant volt-seconds on the Herbert plot—the dashed line in Figure 16. To get power loss from these points, assuming constant frequency of 50 kHz, we then scale these points down by the ratio $2 \cdot t_1/20 \mu\text{s}$ to get the solid line in Figure 16. This rise of this curve to the left illustrated the disadvantage of using shorter duty cycles for a given average voltage or volt-second requirement.

As an asymmetric example, consider the same 12-turn winding, with a 12 V, 10 μs pulse applied in one direction, and a 30 V, 4 μs pulse applied in the other direction, with a 20 μs overall period (50 kHz) as before (the waveform includes a total of 6 μs of zero-voltage time). $P_{\text{sqr}}(V_1/N, t_1)$ and $P_{\text{sqr}}(V_2/N, t_2)$ are read off Figure 15 as 244 mW and 818 mW. The overall power loss can then be found from (3) as

$$P = 50 \text{ kHz} (244 \text{ mW} \cdot 10 \mu\text{s} + 818 \text{ mW} \cdot 4 \mu\text{s}) = 286 \text{ mW}. \quad (5)$$

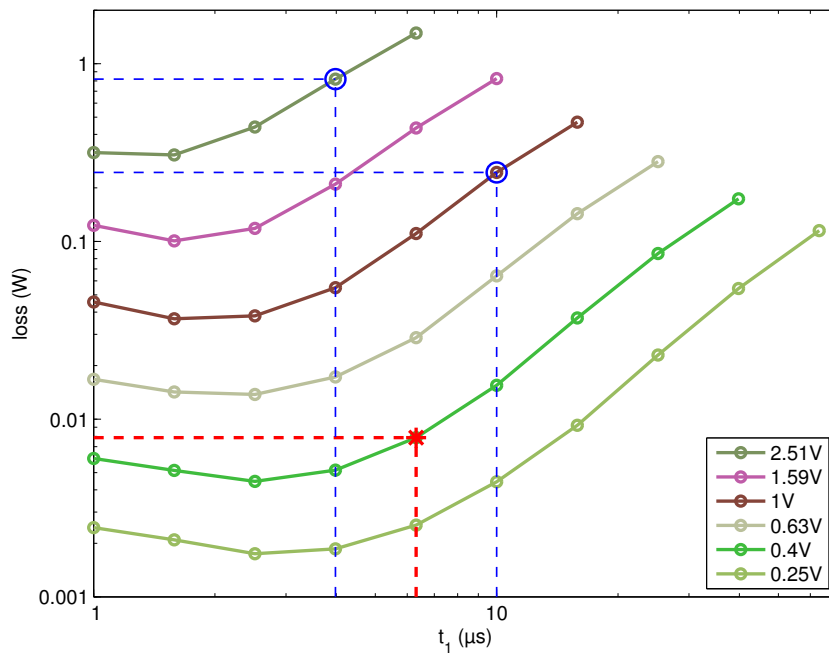


Figure 15: Reading data from a Herbert plot for the examples discussed in the text. The lower red point marked with \star is for the first, symmetric example. The upper blue circles are for the second, asymmetric example.

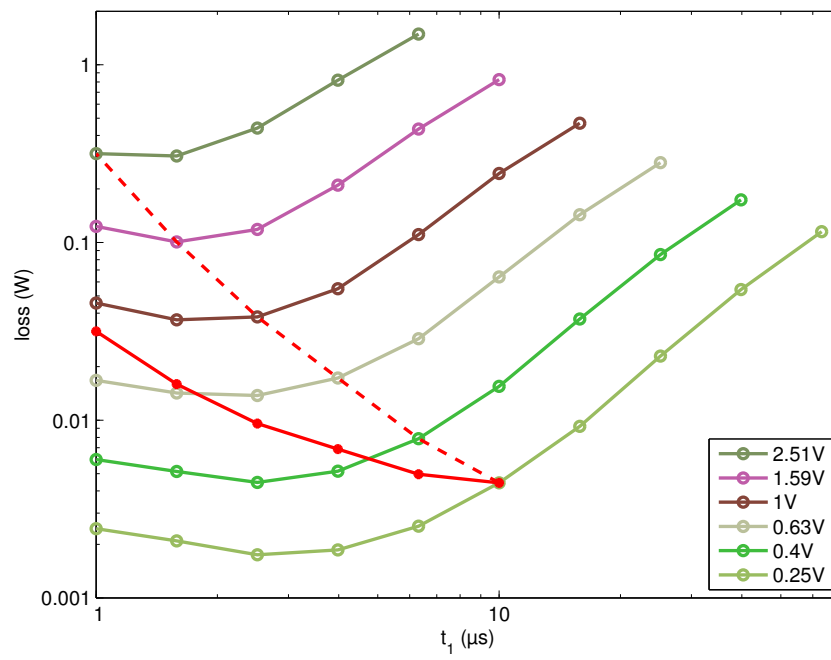


Figure 16: Example exploring different duty cycle options for a constant average voltage (constant volt-seconds). The dashed line is the raw data points used from the plot; the solid line shows the result scaled by the ratio of on-time to period to calculate actual loss, as discussed in the text.

8 Discussion

The results in Figures 8 and 8b show that the composite waveform hypothesis holds well for asymmetric waveforms, and the method provides excellent accuracy. Figure 10 shows that, for the powdered-iron core tested, it also holds very well for waveforms with zero-voltage periods, although zero voltage times can cause significant deviation in the ferrite core tested. This variation is not predicted by the composite-waveform hypothesis; nor is it predicted by any of the methods discussed in Section 2. Additional work to better characterize and model this behavior could lead to more accurate loss predictions. However, even with this error, the approach described here is expected to be more accurate than other methods which are subject to the same error, and additionally entail error due to using sinusoidal data to predict square-wave loss.

In addition to being more accurate than other methods, the new approach is also easier to use than methods like the iGSE. Thus, we believe that it would be beneficial for core manufacturers to characterize square-wave loss and provide that data graphically, electronically or both, either on a per-unit-volume basis or on a per-core basis.

As presented here, the method is only applicable to waveforms with one positive voltage pulse and one negative pulse. However, it could also be easily applied to waveforms with minor loops by separating the minor loops following the approach in [7], as long as each constituent loop comprises only one positive pulse and one negative pulse. Adapting the method to waveforms with a series of voltage pulses of the same polarity but differing amplitudes is less straightforward. The corresponding analysis in the iGSE (eq. (13) in [7]) includes a factor that depends on the total flux excursion as well as the flux change for a given pulse, and it may be necessary to introduce similar factors to accurately model losses in such cases using square-wave loss data. However, most power electronics applications use waveforms with only one positive voltage pulse and one negative pulse, such that the analysis here applies directly.

9 Using the Data

The data generated by this work includes characterization data for two cores and verification data for the same two cores. Complete data for both is archived at the web site <http://engineering.dartmouth.edu/inductor/coredata> in files `ferrite-data.zip` and `powdered_iron-data.zip`. However, a user calculating loss for a particular waveform does not need these large (> 20 MB) files, but rather needs only the characterization data. This data is available in a smaller data collection, `characterization-data.zip`, on the same page. This archive contains the data plotted in Figures 6 and 7 in multiple formats, as well as the plots themselves as Portable Network Graphics (PNG) images. The data include, for each square wave tested,

- Frequency (Hz).
- Peak flux linkage (Vs).
- Volts/turn.
- Average loss (W).
- Loss per cycle (J).

The formats are:

- Microsoft Excel (`.xls`) format, with columns corresponding to each of the data listed above, and headings labeling each.
- Comma-separated value (`.csv`) format, with columns corresponding to each of the data listed above, and no text.
- Plain text (`.dat`) file, with columns corresponding to each of the data listed above, and a header row briefly identifying each column.
- Matlab `.mat` format, which, when loaded into the Matlab environment, provides the variables `f`, `dphi`, `Vturn`, `Pavg`, and `Ecycle`, corresponding to the data listed above.

These formats are explained in greater detail in the appendix.

Many users may wish to simply read values off of the graphs in Figures 6 and 7 but these files make the data available in multiple formats for use by computer software, or for analyzing, curve-fitting, or plotting the data.

10 Conclusion

The proposed measurement and loss calculation approach allows generalizing square-wave core-loss data to predict core loss with any common rectangular voltage waveform. An automated measurement system has been used to collect the required square-wave core characterization data for ferrite and powdered-iron cores, and to collect additional data to assess the accuracy of the method for other voltage waveforms. Measurements show good correlation, but also exhibit behavior not yet explained by published

models, which may lead to new insights and more accurate models. Despite the minor discrepancies, the loss prediction method yields higher accuracy, and is easier to use, than other methods for non-sinusoidal waveforms.

A Data Files and Fields

This appendix summarizes the various field names in the data files, along with their meanings. Table 3 gives a summary of all the files. In these files, we use designations to identify the four waveform types shown in Figure 1b. They are listed in Table 4.

A.1 Oscilloscope Data

The first *two* lines of the oscilloscope CSV files are heading. The first is the field identifier, the second, the units of measure. All the data are floating point numbers. The SYNC and OUT fields are the input to the waveform decoder and are only used for debugging.

x-axis Time, in seconds.

SYNC The sync signal from the arbitrary waveform generator (volts).

OUT The output signal from the arbitrary waveform generator (volts).

V The sense winding voltage, V_s , (volts).

Field	Description
<i>set-gen.dat</i>	The Gen-runs input data file, instructions for making a set of runs.
<i>set-runs.dat</i>	The output from Gen-runs and the input to the Coreloss program.
<i>set-gen.log</i>	A log file from Gen-runs echoing the parameters and telling which runs were skipped and why.
<i>set-log.dat</i>	A diagnostic file created by the Coreloss program.
<i>set-log.csv</i>	A diagnostic file created by the Coreloss program. It has the same informations as the <i>.dat</i> file, above, but in the CSV format.
<i>set-run.csv</i>	The output from the oscilloscope for a single run.
<i>set-run.txt</i>	A configuration log from the oscilloscope for a single run.
<i>set-run.png</i>	An image of a plot of the oscilloscope data for a single run, along with a plot of power and energy versus time.
<i>output.dat</i>	Contains the per-cycle loss data, as well as the original data.
<i>output.csv</i>	Contains the per-cycle loss data, as well as the original data. It has the same informations as the <i>.dat</i> file, above, but in the CSV format.
<i>data.mat</i>	Contains the per-cycle loss data, as well as the original data. It has the same informations as the <i>.dat</i> file, above, but as Matlab source code.

Table 3: File naming conventions for parameter and data files.

Designation	D	$t_1 = t_2$	Symmetric	Comment
square	= 1	yes	yes	
skew	< 1	yes	no	“shifted”
expand	< 1	yes	yes	varying T
assym	= 1	no	no	

Table 4: Waveform type designations

I The current (amperes).

A.2 Test Input Data

The test input file read by the Coreloss program. Each record is a white-space-delimited list of the parameters for one run. An experimental run has these parameters:

runId The run identifier. This should chosen to be globally unique. The Gen-runs program uses the set ID, followed by a zero-padded integer, the run ID.

sample The core sample identifier.

N The number of turns on the core.

period The period, T , of the drive voltage, in seconds. (Floating point.)

t1 The pulse width of the first pulse. (Floating point.)

pinch The *pinch*, P , it the time between pulse 1 and pulse 2, t_0 , expressed as a fraction of the off time for a symmetric waveform:

$$P = 1 - \frac{2t_0}{T - t_1 - t_2}$$

$0 \leq P \leq 1$ for $D < 1$. $P = 1$ for expand waveforms, and is undefined for $D = 1$ (indicated in the file by -1). (Floating point.)

D=1 A Boolean value, true (1) if $D = 1$ and 0 otherwise. This may seem redundant, but it is needed for clarity and safety because of the floating point time parameters.¹

Vps It is the voltage requested from the power supply.

delay A delay between runs to allow for cooling. (Seconds.)

VRange Full scale voltage range setting for the oscilloscope.

IRange Full scale current range setting for the oscilloscope.

The following fields are used by the data reduction programs to group data by families:

¹The name D=1 was chosen for brevity and clarity. I hope the embedded math symbol is not confusing.

TSet Zero if it is not a `square` wave. Otherwise, records with the same value have the same period.

VSet Zero if it is not a `square` wave. Otherwise, records with the same value have the same V_{ps} .

expandSet Zero if it is not an `expand` waveform. Otherwise, records with the same value have the same pulse shape. (Varying t_0 .)

skewSet Zero if it is not a `skew` waveform. Otherwise, records with the same value have the same pulse shape. (Varying P .)

assymSet Zero if it is not a `assym` waveform. Otherwise, records with the same value have the same pulse shape for the t_1 pulse.

A.3 Run Data Generator

The input file for Gen-runs is a white-space-delimited dictionary. The fields are:

comment This is a one-line comment that is printed at the top of the run data file.

setId The set ID is used to name the run data file and is prepended to each run ID. By convention, this is the same as the set identifier used in the source data file names.

sample The identifier for the core sample.

N The number of turns.

types A list of run types to be generated. They can be any of `{square, expand, skew, assym}`.

t1min Minimum pulse width for `square` wave runs.

t1max Maximum pulse width for `square` wave runs.

VpsMin Minimum power supply voltage.

VpsMax Maximum power supply voltage.

grid Spacing of the geometric series, in decilog. For five values per decade, use 2.

satLimit Saturation limit in power supply volt-seconds per turn.

delay The delay time for cooling between runs, in seconds.

expandSamples A white-space-delimited, paired list of V_{ps}/N and t_1 for the pulses used in `expand` and `skew` runs. These values will be “rounded” to the decilog preferred values (Section 4.2).

t0min The minimum off-time between pulses, t_0 , to be used for `expand` and `skew` runs.

t0max For *expand* and *skew* runs, the maximum off-time. *expand* waveforms are symmetric, with the period $T = 2(t_1 + t_0)$. The off time, t_0 , increases geometrically, stopping when it exceeds $t_{0\max}$.

TFactor For *skew* runs, the ratio of the period, T , to the pulse width, used to determine T , i.e., the period is $T_{\text{Factor}} * t_1$. The series starts with $t_0 = t_{0\min}$, and increases t_0 geometrically until the pulses are approximately symmetric.

For comments; both the key (#) and the value are ignored by the program.

B General File Formats

There are a few general types of file format used in the project:

Comma separated value (CSV). This is a standard tabular format, where columns are separated by commas. Files have the `.csv` extension. It was chosen because it was the only ASCII text output file format available from the Tektronix oscilloscope. The first line or two of all the CSV files is a header.

Key-value dictionary. This is a particularly nice, human and machine readable format for configuration files. Each line has zero or more white-space-delimited key-value pairs. The *key* is a unique parameter name; the *value* is the value it is assigned. The layout and order of the pairs is unimportant. If a value is enclosed in quotation marks or braces, it may be empty or contain embedded white space.

Log. Log files are text files and usually have the extension `.log`. They give diagnostic information and are intended for human readers, and are generally not easily parsed by a computer.

White space delimited table. These are ASCII text table files that separate columns with white space—spans of one or more space or tab characters. They are easily read by a human if printed with a monospaced font, like Courier. Cells that are empty, or contain white space, must be enclosed in quotation marks or braces. Blank lines and lines beginning with `#` are ignored. The latter are often used for headings.

Portable network graphic (PNG). These are raster graphics files, used for the data plots.

Matlab MathWorks MATLAB source code file, which have the extension `.mat`.

Acknowledgements

Thanks to the Power Sources Manufacturers' Association and the National Institute for Standards and Technology (NIST) for support of this work.

References

- [1] Edward Herbert. User-friendly data for magnetic core loss calculations. August 2008. <http://fmtt.com/Coreloss2009.pdf>.
- [2] M. Albach, T. Durbaum, and A. Brockmeyer. Calculating core losses in transformers for arbitrary magnetizing currents a comparison of different approaches. In *27th Annual IEEE Power Electronics Specialists Conference*, volume 2, pages 1463–8, June 1996.
- [3] J. Reinert, A. Brockmeyer, and R.W. De Doncker. Calculation of losses in ferro- and ferrimagnetic materials based on the modified Steinmetz equation. In *Proceedings of 34th Annual Meeting of the IEEE Industry Applications Society*, pages 2087–92 vol.3, 1999.
- [4] A. Brockmeyer. *Dimensionierungswerkzeug für magnetische Bauelemente in Stromrichteranwendungen*. PhD thesis, Aachen University of Technology, 1997.
- [5] Jinjun Liu, T. G. Wilson, Jr., R. C. Wong, R. Wunderlich, and F. C. Lee. A method for inductor core loss estimation in power factor correction applications. In *Proceedings of APEC 2002—Applied Power Electronics Conference and Exposition*, page 439, 2002.
- [6] Jieli Li, T. Abdallah, and C. R. Sullivan. Improved calculation of core loss with nonsinusoidal waveforms. In *IEEE Industry Applications Society Annual Meeting*, pages 2203–2210, 2001.
- [7] K. Venkatachalam, C. R. Sullivan, T. Abdallah, and H. Tacca. Accurate prediction of ferrite core loss with nonsinusoidal waveforms using only Steinmetz parameters. In *IEEE Workshop on Computers in Power Electronics*, 2002.
- [8] A.P. Van den Bossche, D.M. Van de Sype, and V.C. Valchev. Ferrite loss measurement and models in half bridge and full bridge waveforms. In *IEEE Power Electronics Specialists Conference*, pages 1535–1539, June 2005.
- [9] Alex van den Bossche and Vencislav Valchev. *Inductors and Transformers for Power Electronics*. Taylor and Francis Group, 2005.
- [10] S. Mulder. Power ferrite loss formulas for transformer design. *Power Conversion & Intelligent Motion*, 21(7):22–31, July 1995.
- [11] E. C. Snelling. *Soft Ferrites, Properties and Applications*. Butterworths, second edition, 1988.

- [12] C. P. Steinmetz. On the law of hysteresis. *AIEE Transactions*, 9:3–64, 1892. Reprinted under the title “A Steinmetz contribution to the ac power revolution”, introduction by J. E. Brittain, in *Proceedings of the IEEE* 72(2) 1984, pp. 196–221.
- [13] A. Brockmeyer. Experimental evaluation of the influence of dc-premagnetization on the properties of power electronic ferrites. In *APEC '96. Eleventh Annual Applied Power Electronics Conference*, pages 454–60, 1996.
- [14] A. Brockmeyer and J. Paulus-Neues. Frequency dependence of the ferrite-loss increase caused by premagnetization. In *Twelfth Annual Applied Power Electronics Conference and Exposition*, pages 375–80, 1997.
- [15] Wai Keung Mo, D.K.W. Cheng, and Y.S. Lee. Simple approximations of the dc flux influence on the core loss power electronic ferrites and their use in design of magnetic components. *IEEE Transactions on Industrial Electronics*, 44(6):788–99, 1997.
- [16] G. Bertotti. General properties of power losses in soft ferromagnetic materials. *IEEE Transactions on Magnetics*, 24(1):621–630, 1988.
- [17] G. Bertotti. *Hysteresis in magnetism: for physicists, materials scientists, and engineers*. Academic Press, 1998.
- [18] K. H. Carpenter. Simple models for dynamic hysteresis which add frequency-dependent losses to static models. *IEEE Transactions on Magnetics*, 34(3):619–22, 1998.
- [19] J.-T. Hsu and K. D. T. Ngo. A Hammerstein-based dynamic model for hysteresis phenomenon. *IEEE Transactions on Power Electronics*, 12(3):406–413, 1997.
- [20] H. Saotome and Y. Sakaki. Iron loss analysis of Mn-Zn ferrite cores. *IEEE Transactions on Magnetics*, 33(1):728–34, 1997.
- [21] W. Roshen. Ferrite core loss for power magnetic components design. *IEEE Transactions on Magnetics*, 27(6):4407–15, 1991.
- [22] P. Tenant and J. J. Rousseau. Dynamic model of magnetic materials applied on soft ferrites. *IEEE Transactions on Power Electronics*, 13(2):372–9, 1998.
- [23] F. Fiorillo and A. Novikov. An improved approach to power losses in magnetic laminations under nonsinusoidal induction waveform. *IEEE Transactions on Magnetics*, 26(5):2904–10, 1990.
- [24] D. C. Jiles. Frequency dependence of hysteresis curves in ‘non-conducting’ magnetic materials. *IEEE Transactions on Magnetics*, 29(6):3490–2, 1993.
- [25] Wei Shen, Fei (Fred) Wang, Dushan Boroyevich, and C. Wesley Tipton. Loss characterization and calculation of nanocrystalline cores for high-frequency magnetics applications. *IEEE Transactions on Power Electronics*, 23(1), 2008.

- [26] Ray Ridley and Art Nace. Modeling ferrite core losses. *Switching Power Magazine*, 3(1):6–13, 2002.
- [27] Christopher Oliver. A new core loss model. *Switching Power Magazine*, 3(2), 2002.
- [28] Ferrite material selection guide, 2000. Magnetics Division of Spang & Company, Bulletin No. FC-S1.
- [29] Soft ferrites and accessories, data handbook, 2009. Ferroxcube, Eindhoven, The Netherlands.
- [30] Ferrites and accessories: SIFERRIT materials, 2006. EPCOS AG, Munich, Germany.
- [31] K. H. Carpenter and S. Warren. A wide bandwidth, dynamic hysteresis model for magnetization in soft ferrites. *IEEE Transactions on Magnetics*, 28(5):2037–41, 1992.
- [32] I. D. Mayergoyz. *Mathematical models of hysteresis*. Springer-Verlag, 1991.
- [33] Ping Han, G. R. Skutt, Ju Zhang, and F. C. Lee. Finite element method for ferrite core loss calculation. In *Applied Power Electronics Conference and Exposition*, volume 1, pages 348–353, 1995.

User-friendly Data for Magnetic Core Loss Calculations

Edward Herbert, Canton, CT.

November 10, 2008

Introduction:

Everyone "knows" that core losses depend only upon \hat{B} and frequency. It does not matter what the excitation level and duty-cycle is, only the maximum flux density \hat{B} . That is true, if the switching frequency is below 10 kHz or so. At the frequencies used in today's pulse-width-modulated (pwm) transformers, the core losses increase dramatically for low duty-cycles, as much as 10 times at 10 % duty-cycle.

Graphs of magnetic core loss data are usually for sine-wave excitation and presented in terms of maximum flux density \hat{B} and frequency f . These graphs are of questionable value for pulse-width-modulated (pwm) power converter design and decidedly not user-friendly. Graphs of core loss data for square-wave excitation, presented in terms of applied voltage and time are much more relevant to pwm power converter design and are much easier to use.

Background:

Magnetic core loss graphs from manufacturers are marginally useful for pwm power converter design. (1) They usually present loss in terms of maximum flux density \hat{B} , an unfamiliar parameter of little use to the power converter designer. (2) The magnetic units used for core loss graphs are confusing and inconsistent. The likelihood of making errors is significant. (3) The graphs are for sine-wave excitation. Most pwm converters

operate with square-waves having a variable duty-cycle. (4) The graphs are notoriously inaccurate. It is not unusual to see ruler-straight lines on core loss curves, with gross inaccuracies at the extremes.

Some very interesting work has been done exploring losses at increased "effective frequency." [1], [2] and [3].

Using volt-second graphs

Figure 1 shows representative core loss curves for square-wave excitation, presented as a family of constant voltage curves vs. pulse-width t .

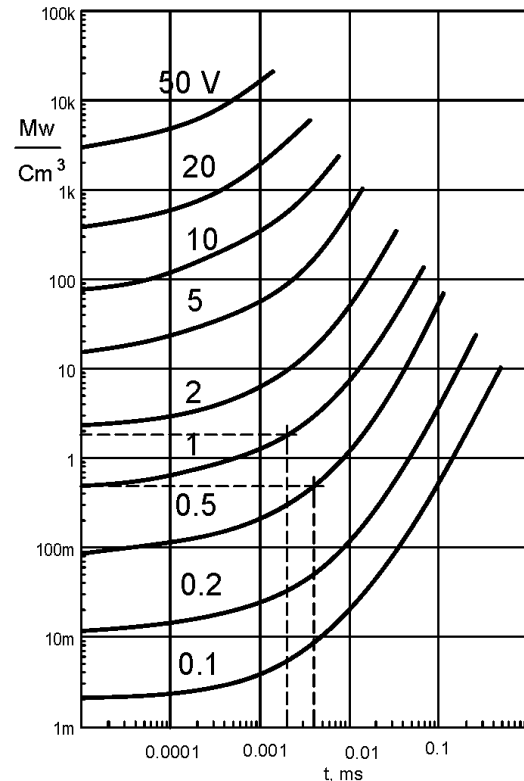


Figure 1: Representative core loss curves for constant voltage square-wave excitation vs. pulse-width.

For a graph for a magnetic material, the voltage is normalized and has units of volts per area-turn and the loss is in watts per volume. Core loss graphs for specific cores can include the geometric parameters, so the units are volts/turn and watts.

Low duty-cycle data

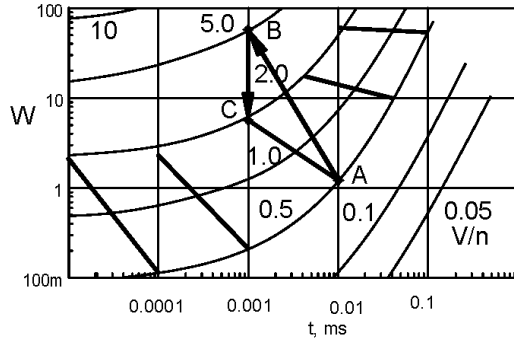


Figure 2. Curves of constant average voltage can be plotted. Note the extreme change in slope for short pulse widths (high frequency).

In figure 2, curves of constant average voltage equal to 0.5 V were plotted for several frequencies. As an example, using the technique for low duty-cycles presented below, start with the 0.5 V line and 0.01 ms, point A. That is the loss for a square wave with 0.01 ms pulse width. At 0.001 ms, to have the same average voltage, the voltage during the pulse is 5.0 V, point B, reduced by the duty-cycle 0.1, point C. The line A-C is approximately the line showing the loss for constant average voltage. This may be the most useful curve of all for a power converter designer.

The same technique is repeated to estimate the losses at constant average voltage for other starting pulse-widths (frequencies), resulting in a family of curves, shown in figure 2.

Note that at short pulse-widths (high frequency), the losses rise significantly at low duty-cycle. At longer pulse-widths, (low frequency), the duty-cycle does not much affect losses. This latter case is the classic loss characteristic taught for magnetic design.

The reader is advised that these curves were derived using Steinmetz equations applied far beyond their limits of reasonable accuracy, using many complex manipulations, each an opportunity for error. Accordingly, the graphs are qualitative at best.

However, the graphs represent a suggested form to use for plotting "real" data, from laboratory test and measurement. Real data from real tests will always trump manipulated data and approximations.

This presentation of the data is user-friendly and much more meaningful for power converter design.

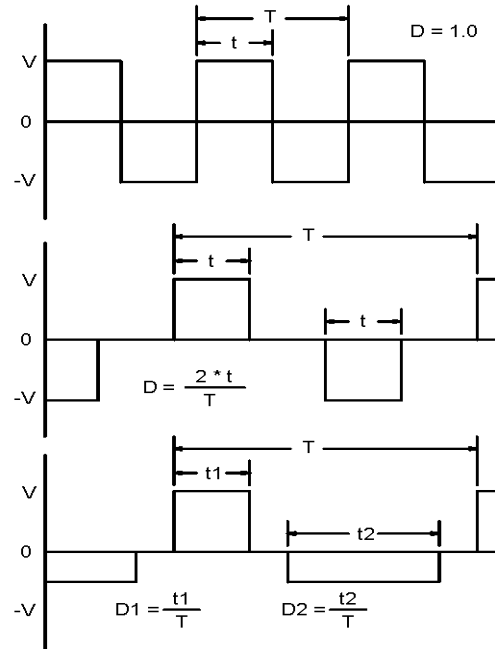


Figure 3: Times and duty-cycles defined.

Calculations

See figure 3 to define pulse-width and duty-cycle: In all cases, the pulses are repetitive steady-state pulses, as would be generated in a pwm converter at steady-state conditions.

For a square-wave excitation, t is the pulse-width and T is the period. The duty-cycle D is 1.0 . To calculate the core losses using figure 1 for a 1 volt square-wave with a pulse-width of 2 us, follow the dashed line up from 2 us to intercept the 1 volt curve, then horizontally to intercept the vertical axis. The result is about 1.8 mw/cm^3 .

For a symmetrical pulsed excitation, t is the pulse-width and T is the period. The duty-cycle D is $2 * t / T$. To calculate the core loss for a 1 volt pwm wave-form having a 1 volt excitation and a 2 us pulse-width and a duty-cycle of 0.5, follow the dashed line up from 2 us to intercept the 1 volt curve, then horizontally to intercept the vertical axis. The result is multiplied by the duty-cycle 0.5 to give about 0.9 mw/cm^3 .

For an asymmetrical pulsed excitation, the volt-seconds none-the-less must be equal for the pulses. T is the period, $t1$ is the positive pulse-width, $t2$ is the negative pulse-width. Two duty-cycles are defined, $D1 = t1 / T$ and $D2 = t2 / T$.

To calculate the core loss for an asymmetrical pwm having a period of 8 us, and having a 2 us positive pulse of 1 volt and a 4 us negative pulse of 0.5 volt, first follow the dashed line up from 2 us to intercept the 1 volt curve, then horizontally to intercept the vertical axis. The result is multiplied by the duty-cycle of 0.25 to give about 0.45 mw/cm^3 .

Next, follow the dashed line up from 4 us to intercept the 0.5 volt curve, then horizontally to intercept the vertical axis. The result is multiplied by the duty-cycle of 0.5 to give about 0.24 mw/cm^3 . Add the partial results. The core loss is about 0.69 mw/cm^3 .

Thus a method of calculating core loss is presented that does not require calculating magnetic parameters. This data and the calculations are much more relevant to power converter design, and much more user-friendly.

Saturation

Following the constant voltage curves from left to right, the volt-seconds of each point is the product of the voltage and the pulse-width. The curve ends at the volts-seconds where the core saturates. Accordingly, as long as the voltage and pulse-widths of interest are on the curve, the core will not saturate (if there is no flux walking.)

Loss data for cores and wound components

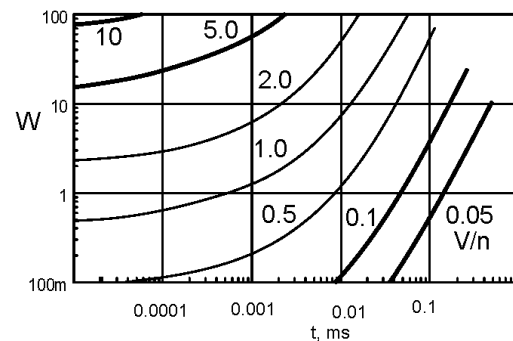


Figure 4. For a specific core, the geometric parameters can be included, so the result is read directly as watts W.

Losses for cores: A manufacturer of magnetic cores can present data for any specific core with all of the geometric

parameters included, so the user need not be concerned with effective area, effective volume and the like. Knowing the volts/turn and the pulse-widths of interest, the losses in the core can be read directly from the graph, as seen in Figure 4.

Losses for wound components: A similar graphical presentation includes the turns, allowing a designer to determine the core losses directly using only the voltage and pulse-widths.

"Remagnetization velocity"

Many papers have suggested that dB/dt and B are more relevant to core loss, leading to improved methods of calculation that have a better match to test data. None, as far as we know, has recognized dB/dt as voltage (with a scale factor). Yet, for most power converter designers, voltage is a much easier parameter to use and understand.

All continue to use maximum flux density \widehat{B} and frequency f . [1] uses the term "remagnetization velocity" for dB/dt . In [2] and [3], the more straightforward " dB/dt " is used.

For any expression using the flux density B or the maximum flux density \widehat{B} , an equivalent expression can be written substituting volt-seconds, with an appropriate scale factor.

"Effective frequency"

[1], [2] and [3] all use the concept of "effective frequency" to account for non-sinusoidal wave-forms. Intuitively, there is a relationship between "duty-cycle" and "effective frequency," duty-cycle being analogous to the ratio of the real frequency to the effective frequency.

For any expression using frequency, an equivalent expression can substitute the inverse of the period, noting that frequency f equals $1/T$, where T is the period. We prefer using the half-cycle period t , so f equals $1/2t$.

Steinmetz equation using voltage v and the period T

The Steinmetz equation (or any other expression using \widehat{B} and f) can be expressed in terms of voltage and time.

$$P_v = C_m * f^\alpha * \widehat{B}^\beta$$

Substituting $f = 1/T$
and $\widehat{B} = k * v * T$ gives

$$P_v = C_m * \left(\frac{1}{T}\right)^\alpha * (k * v * T)^\beta$$

$$P_v = C'_m * v^\beta * T^{(\beta-\alpha)}$$

[T is the period, k is the scale factor converting volt-seconds to \widehat{B} , v is the voltage density and $C'_m = C_m * k^\beta$.]

This exercise is to demonstrate the equivalence of the expressions, not to suggest converting present data to the new format, particularly as we prefer using square-wave excitation. New data should be taken using voltage and pulse-width.

Graphs using converted data

To illustrate the point, we converted data mathematically to make the graphs that follow.

The starting point is the data as they are usually presented for Magnetics, Inc. F material. These data were chosen because Magnetics, Inc. also provides a family of Steinmetz constants for the F

material, as shown in the box below [6]. The frequency ranges are colored and correspond with the colors of the curves in the graphs.

Figure 5 shows a composite graph, taking the data for the F material from a data sheet (the solid lines) and superimposing on it the curves resulting from the Steinmetz calculations (the dashed lines).

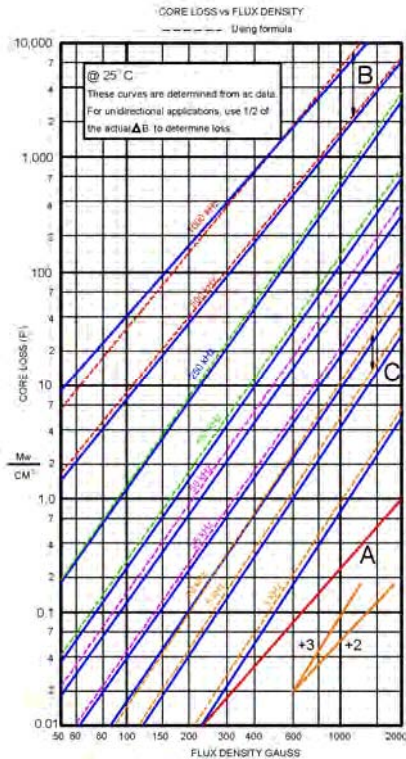


Figure 5: Core loss data for Magnetics, Inc. material F. The solid lines are from the datasheet, and the dashed lines are calculated using the Steinmetz equations.

Magnetics, Inc.'s loss expression approximation is:

$$P_L = a * f^c * \hat{B}^d \text{ mW/cm}^3$$

[Where a , c and d are constants, f is in kHz and \hat{B} is in kG.]

For each line in figure 3, the slope of the line is the exponent d , and the spacing between the lines is governed by the exponent c .

Core loss vs. frequency.

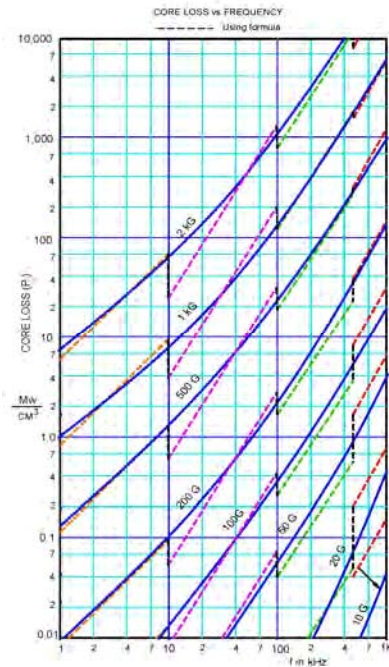


Figure 6: The data for Magnetics Inc. material F was re-plotted as a family of curves of constant flux density vs. frequency.

For Magnetics Inc.'s F material, the Steinmetz constants are given as follows.

Range	a	c	d
$f \leq 10 \text{ kHz}$	0.790	1.06	2.85
$10 \text{ kHz} \leq f < 100 \text{ kHz}$	0.0717	1.72	2.66
$100 \text{ kHz} \leq f < 500 \text{ kHz}$	0.0573	1.66	2.68
$f \geq 500 \text{ kHz}$	0.0126	1.88	2.29

The colors correspond to frequency ranges in the graphs.

First, the data was re-plotted using curves of constant \hat{B} vs. f as in figure 6. Note the extreme discontinuities in the calculated data (dashed lines). These lines should be continuous, pointing out dramatically how poor the Steinmetz approximation is at the extremes of the frequency ranges. The solid lines are drawn free-hand in an attempt to find the best fit through the calculated data.

Excitation voltage vs. frequency

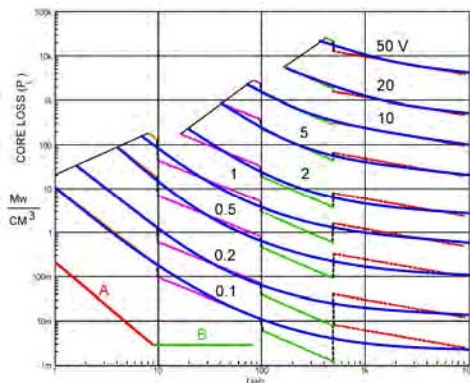


Figure 7: The data are re-plotted as a family of curves of constant excitation vs. frequency.

Next, the data is plotted in terms of voltage and frequency. This required substituting volt-seconds (with a scale factor) for \hat{B} , but then substituting back the frequency f term as the inverse of the seconds. The result is a family of loss curves of the excitation voltage (in volts/turn-cm²) vs. frequency, as shown figure 7.

Again, the dashed lines are the calculated curves, and the solid lines are a "best fit" drawn free-hand. On the upper left, the lines were ended at a flux density of 3 kG. This would be a straight line if the equations were ideal.

Voltage vs. pulse-width

The final translation is to re-plot the curves in terms of pulse-width rather than frequency. Because the pulse-width t is used instead of the period T , the scale was shifted left by 2. Only the "best fit" curves were used. The graph in figure 8 was rescaled to square up the log-log coordinates, and possible asymptotes of the curves were added. With further editing for appearance, this graph became the graph of figure 1.

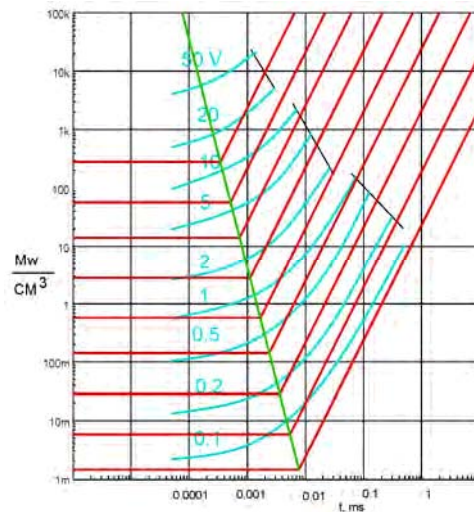


Figure 8: The curves of figure 7 were flipped left to right to invert the frequency scale to a time scale, and it was shifted left by 2 so that the scale is pulse-width t rather than the period T .

While this graph was derived from data for the Magnetics, Inc. F material, the reader is reminded that curves are based upon the Steinmetz equations applied far beyond their range of reasonable accuracy. The complexity of the calculations makes the chance of error quite significant. As such, only qualitative relationships can be inferred.

However, new data taken using square-wave constant voltage excitation and presented as a function of the pulse-width (half period) of the square-wave

will be no less accurate and valid than the data presently used, while being much more relevant to power converter design and much more "user-friendly."

Steinmetz-like equations

Rather than try to shoe-horn the Steinmetz factors into a new form, it is suggested that a new Steinmetz-like equation be defined.

$$P_v = C_x * v^\delta * t^\epsilon$$

Find the area on the graph over which the circuit of interest will operate, and pick three points that bracket that area. For each, write the Steinmetz-like equation, with the constants as unknowns, and solve the equations simultaneously. Since solving simultaneous equations in which two of the unknowns are exponents is daunting, it is suggested to use a math program such as MathCad.

Oliver-like equations and Ridley-Nace-like equations

In [4], Christopher Oliver presents a curve fitting algorithm that is accurate over a much broader area of the graph. In [5], Dr. Ray Ridley and Art Nace do the same (but with a much different algorithm), and introduce temperature compensation as well. We see no reason why similar techniques could not be applied to voltage and pulse-width graphs as well, as the underlying physics is the same.

Conclusion

Core loss data can be taken for square-wave excitation, and presented in terms

of the excitation voltage and pulse-width with no loss in accuracy.

Core loss data can also be taken and presented as curves of constant average voltage vs. pulse width, to show the consequence of low duty-cycle operation.

The resulting data are much more relevant to pwm power converter design, and are much more "user-friendly".

References

- [1] Ansgar Brockmeyer, Manfred Albach, and Thomas Dürbaum, *Remagnetization Losses of Ferrite Materials used in Power Electronic Applications*, Power Conversion, May 1996 Proceedings.
- [2] Jeili Li, Tarek Abdallah and Charles R. Sullivan, *Improved Calculation of Core Loss with Nonsinusoidal Waveforms*, IAS 2001.
- [3] Kapil Venkatachalam, Charles R. Sullivan, Tarek Abdallah and Hernán Tacca, *Accurate Prediction of Ferrite Core Loss with Nonsinusoidal Waveforms Using Only Steinmetz Parameters*, COMPEL 2002
- [4] Christopher Oliver, *A new Core Loss Model*, Switching Power Magazine, Spring 2002.
- [5] Dr. Ray Ridley and Art Nace, *Modeling Ferrite Core Losses*, Switching Power Magazine © Copyright 2006.
- [6] Magnetics, Inc. *Ferrite Cores Design Manual and Catalog*, 2006.